

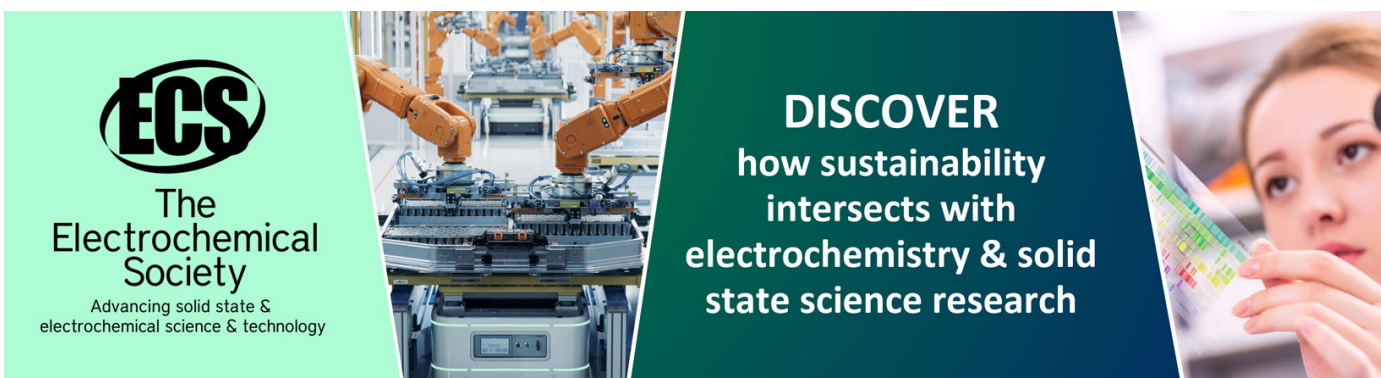
Modeling mechanical energy storage in springs based on carbon nanotubes

To cite this article: F A Hill *et al* 2009 *Nanotechnology* **20** 255704

View the [article online](#) for updates and enhancements.

You may also like

- [Complete mineralization of a humic acid by \$\text{SO}_4^{2-}\$ generated on \$\text{CoMoO}_4/\text{qC}_3\text{N}_4\$ under visible-light irradiation](#)
Zhao Gao, Hanpei Yang, Yang Cao et al.
- [Enhanced current rectification in graphene nanoribbons: effects of geometries and orientations of nanopores](#)
Joydeep Majhi, Santanu K Maiti and Sudin Ganguly
- [Synergy effect in hybrid nanocomposites based on carbon nanotubes and graphene nanoplatelets](#)
Audrey Gbaguidi, Sirish Namilaie and Daewon Kim



ECS
The
Electrochemical
Society
Advancing solid state &
electrochemical science & technology

DISCOVER
how sustainability
intersects with
electrochemistry & solid
state science research

Modeling mechanical energy storage in springs based on carbon nanotubes

F A Hill, T F Havel and C Livermore

Department of Mechanical Engineering, MIT, Cambridge, MA, USA

Received 12 February 2009, in final form 10 April 2009

Published 3 June 2009

Online at stacks.iop.org/Nano/20/255704

Abstract

A modeling study of the potential for storing energy in the elastic deformation of springs comprised of carbon nanotubes (CNTs) is presented. Analytic models were generated to estimate the ideal achievable energy density in CNTs subject to axial tension, compression, bending and torsion, taking into account limiting mechanisms such as the strength of individual CNTs, the onset of buckling, and the packing density limitations of CNT groupings. The stored energy density in CNT springs is predicted to be highest under tensile loading, with maximum values more than three orders of magnitude greater than the energy density of steel springs, and approximately eight times greater than the energy density of lithium-ion batteries. Densely packed bundles of precisely aligned, small diameter single-walled carbon nanotubes are identified as the best structure for high performance springs. The conceptual design and modeling of a portable electric power source that stores energy in a CNT spring are presented as tools for studying the potential performance of a system for generating electricity from the CNTs' stored mechanical energy.

1. Introduction

There exists a growing need for rechargeable, high energy density energy storage media for use in small, lightweight, highly efficient portable power sources. This paper presents a study of the potential and feasibility of using mechanical springs comprised of carbon nanotubes (CNTs) for energy storage. To use a CNT spring as an energy storage medium, the spring must first be deformed elastically in order to store energy in the structure's deformation. The spring would then be latched in its deformed configuration in order to hold the stored energy in the system until use. Finally, the spring's deformation would be relaxed, transmitting the stored energy to the desired load in the process. The application of CNTs to mechanical energy storage is motivated by the exceptional properties of individual CNTs, which include high stiffness, high strength, high flexibility, and low density [1]. Since the maximum stored energy density of a linear elastic material is proportional to the product of its material stiffness and the square of its maximum elastic strain, springs based on dense arrays of CNTs are an ideal medium for reversible mechanical energy storage.

Considerable work has been done previously to characterize the mechanical properties of CNTs experimentally. The effective Young's modulus of single-walled CNTs (SWCNTs) and multi-walled CNTs (MWCNTs) is usually estimated to

be 1 TPa, assuming a wall thickness of 0.34 nm [1]. Elastic strains of up to 6% have been demonstrated experimentally to date [2], while molecular dynamics models predict reversible tensile strains as high as 20% [3–5]. CNTs are highly flexible and are able to withstand significant compression, elongation, twisting and bending in a reversible manner and without inducing fracture or plastic deformation [6, 7]. Although some materials offer a subset of these characteristics, it is the combination of high flexibility, high strength and high stiffness that distinguishes CNTs from other materials as an energy storage medium. Of course, the use of CNTs for their mechanical properties is not new; for example, CNTs have been randomly dispersed into matrix materials as a low-volume-fraction reinforcement to create a composite with higher modulus, strength and toughness than the matrix alone [8]. In contrast, the present work examines the use of materials that are completely or predominantly composed of highly ordered arrays of CNTs for energy storage.

While impressive mechanical properties have been recorded for individual CNTs, the ability to fabricate macroscale fibers and yarns made of millions or more CNTs with comparable properties remains elusive. The challenge lies in the difficulty of controlling the alignment, degree of entanglement, packing density, defects and presence of nanoscale impurities within macroscale assemblies. The strength and stiffness of the best fibers and yarns demonstrated

to date are more than an order of magnitude lower than the ideal values of individual CNTs [9, 10]. The present work examines the energy densities for individual CNTs under a range of deformations. This provides an upper bound for the energy densities of CNT arrays and predicts their performance in the case that the assembly maintains the properties of individual CNTs.

High energy density is just one of many potential benefits of CNT springs as an energy storage medium. Because spring-based energy storage is based on different physics than that which governs electrochemical batteries, the operational characteristics and limitations of such a device will be different from those of batteries. For example, batteries operate with their best energy density when they are discharged slowly; in contrast, springs can release their energy quickly without great loss of efficiency. In addition, because stretching chemical bonds by deforming a macroscale spring is inherently a more controllable and reversible process than most chemical reactions, which break and reform bonds, an energy storage medium based on CNT springs offers the potential for a much greater number of charge–discharge cycles, less self-discharge, less sensitivity to temperature and other environmental conditions, and perhaps even safer operation than electrochemical batteries. Finally, in systems such as regenerative braking for vehicles where the target load is mechanical rather than electrical, mechanical energy storage may be a simpler and more efficient solution than batteries coupled to motor/generators.

Practical considerations also play a role in assessing the potential of CNT springs for implementation as an energy storage medium. One consideration is the ability to synthesize long, low-defect CNTs that are suitable for incorporation into CNT springs in large quantities and at relatively low costs. Recent progress in this area includes the synthesis of CNTs with lengths at the centimeter scale [11]. A second consideration is the ability to create microscopically highly ordered, macroscale CNT assemblies that can store significant amounts of energy and be controlled more easily than individual CNTs; recent research on creating increasingly strong carbon nanotube fibers provides a useful starting point [10, 12]. A third consideration is that a practical system will require not just the CNT springs themselves, but also other structures with which to control the spring deformation; the mass and volume of these ancillary structures will reduce the overall energy density of the system. In particular, a supporting structure must be employed to carry the load of the deformed CNT spring while energy is stored in it, and a practical system must also include a coupling mechanism to transfer the stored energy to the external load. The overall stored energy density of the system will therefore be lower than the energy density of the CNT springs themselves, and the extractable energy density (after losses due to less than ideal efficiencies) will be lower still.

This paper examines these issues in detail in order to assess the potential of CNT springs for energy storage. Section 2 presents energy density estimates for CNTs under different modes of mechanical deformation, and then extends these estimates to include the effect of a support structure

on the overall energy density. Section 3 presents the design and modeling results for a conceptual power source that incorporates a CNT-based spring. The model predicts the power output, overall system efficiency, operating frequency of the energy regulation mechanism, and energy discharge time. Finally, section 4 outlines the implications of these results for the development of practical energy storage devices that use CNT-based springs.

2. Energy density

In this work, well-established, analytical models for CNT mechanics were utilized to estimate the energy that may be stored in elastically deformed CNT springs under a broad range of different loading conditions. The value of this modeling approach lies in the simplicity and computational efficiency with which it provides guidance for the design of CNT-based springs and energy storage systems. Ideally, such analytical models provide insight into the physical trends that govern the potential performance of this proposed new type of energy storage system. The insights gained in this way may then be used to design specific energy storage systems, which may then be further studied by more advanced numerical analyses and ultimately by experiments.

The analytical models used here employ several approximations. The CNTs are modeled using the continuum assumption [8], in which each CNT is treated as a uniform, hollow, cylindrical beam, and each shell of the CNT is taken to contribute 0.34 nm to the beam's wall thickness. Therefore, each beam has an inner radius r_i , a tightly packed wall thickness of $n \cdot 0.34$ nm, and an outer radius $r_o = r_i + n \cdot 0.34$ nm, where n is the number of shells in the CNT. The model does not account for sets of diameters of the internal MWCNT shells other than the tightly packed structure described above because non-tightly packed MWCNTs would buckle more easily and would in general have lower spring performance than otherwise identical, tightly packed MWCNTs would. The commonly accepted Young's modulus E of 1 TPa is employed [1]. The maximum deformations are assumed to be governed by either the elastic limit or the onset of buckling, depending on which limit is reached first. Treating a CNT as a beam is a simplistic model that does not account for the nested shell structure, van der Waals forces, shear interactions between the layers, or non-linear post-buckling behavior [13]. However, because the simple analytical models used here employ parameters derived from more advanced analytical models such as molecular dynamics, they provide reasonable strain energy density estimates in the elastic regime and before the onset of buckling. Finally, the maximum gravimetric energy density of a spring comprising a large assembly of CNTs under a given mode of deformation is assumed to be equal to the maximum gravimetric energy density of a single CNT under that deformation. In practice, some modes of deformation are more readily applied to all members of an assembly in a uniform fashion than others, so this assumption will generally produce an upper bound on the maximum energy density that may be stored in the assembly. Using these assumptions, the strain energy density is

estimated in CNT springs under loading in axial tension, axial compression, bending, and torsion.

In continuum mechanics, the energy stored in an elastically deformed object is given by

$$U = \frac{1}{2} \int_V \sum_i \sum_j \sigma_{ij} \varepsilon_{ij} dV \quad (1)$$

where V is the volume of the body, σ is the stress tensor, and ε is the strain tensor. For the case of CNTs loaded below the failure and/or buckling limits in axial tension or axial compression to an elastic strain of ε , the volumetric energy density u_v^{shells} within the shell walls (i.e. omitting the unfilled space inside the CNT from the volume integral) is given by

$$u_v^{\text{shells}} = \frac{1}{2} E \varepsilon^2, \quad (2)$$

while the gravimetric energy density u_m^{shells} within the shell walls is given by

$$u_m^{\text{shells}} = \frac{1}{2} E \varepsilon^2 \frac{1}{\rho} \quad (3)$$

where ρ is the density. The existence of unfilled space inside a CNT (and between the CNTs that comprise a CNT assembly) will not affect gravimetric energy density, so the overall gravimetric energy density u_m will be equal to the gravimetric energy density u_m^{shells} of the shells alone. However, the unfilled space does impact the volumetric energy density of the overall structure, so that the overall volumetric energy density of the spring u_v will not be equal to the volumetric energy density u_v^{shells} of the shells. Approximating a CNT as a cylindrical tube, its cross-sectional area is $A = \pi(r_o^2 - r_i^2)$, and its total enclosed area is $A_{\text{encl}} = \pi r_o^2$. Therefore, the overall strain energy density per unit volume of a hollow cylindrical beam loaded to an elastic axial strain of ε under axial tension or compression is reduced by a factor of A/A_{encl} , yielding.

$$u_v = \frac{1}{2} E \varepsilon^2 \frac{A}{A_{\text{encl}}}. \quad (4)$$

For springs composed of large assemblies of CNTs, the overall volumetric energy density u_v of the spring will be reduced further by the spacing between the CNTs in the assembly. The amount of spacing will depend on the size, uniformity, and packing of the CNTs. For CNTs packed into an ideal hexagonal lattice, the spacing between adjacent CNTs will be 0.34 nm [1]. This reduces u_v by an additional fill factor $f = 0.91$ [14].

Equation (4) assumes effective load transfer through all shells of a tightly packed MWCNT. For ideal MWCNTs (that is, those in which the inter-shell coupling is solely due to van der Waals effects), the assumption that all shells fully share the load is only valid under compressive loading or bending. It is not valid for ideal, tightly packed MWCNTs under tensile or torsional loading because the inner shells slide past one another almost without friction [15, 16]. For an ideal MWCNT under tensile or torsional loading, the outer shell carries most of the load, so that the maximum achievable strain energy density for ideal MWCNTs in tension or torsion will be significantly reduced as compared with the case in which all

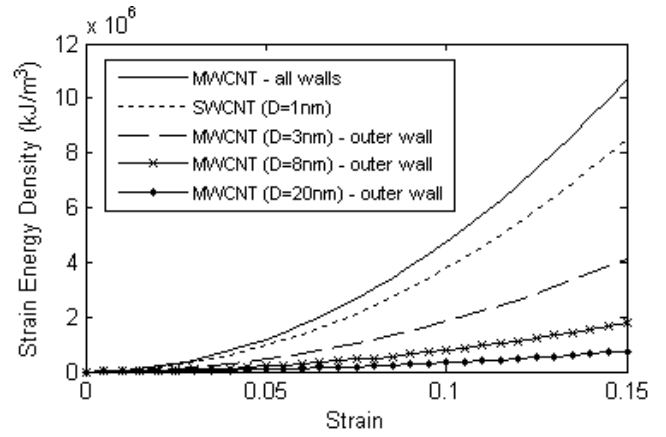


Figure 1. Volumetric energy density as a function of tensile strain for SWCNTs and MWCNTs.

shells carry the load. However, previous work has shown that inter-shell interactions in MWCNTs are not necessarily ideal. In particular, the existence of inter-shell sp³ bonds, which may be created using controlled sputtering or irradiation, can significantly improve inter-shell load transfer [17]. In this case, it may be possible to transfer loads to the inner shells of the MWCNT, though the induced defects may decrease the axial strength.

Figure 1 plots the calculated volumetric energy density u_v (equation (4)) as a function of axial strain for the tensile loading both of SWCNTs and of MWCNTs with either just the outer shell carrying the load (to represent ideal MWCNTs) or all shells carrying the load (as an absolute upper bound on MWCNTs with inter-shell load transfer). The SWCNTs' diameter is taken to be 1 nm, and the MWCNTs' outer diameters are taken to be 3, 8 and 20 nm. In the case where all MWCNT shells carry the load, the MWCNTs are assumed to be entirely filled with densely packed inner shells to determine the upper bound on the energy density; under this assumption, the volumetric energy density of MWCNTs in which all shells carry the load does not depend on the outer diameter. The energy density is maximized by applying high tensile strains to the spring; the strain that can be applied to the spring in tension is limited only by the elastic limit. The ratio A/A_{encl} must be large to achieve high energy density, so assemblies of SWCNTs with small diameters offer higher energy density than do MWCNTs in which only the outer shell carries a tensile load. Defect-free, densely packed, completely filled MWCNTs in which all shells carry the load offer a somewhat higher value of maximum energy density than that offered by small diameter SWCNTs. This energy density represents an upper bound on MWCNT performance because it assumes that there is complete load transfer between shells but that the defects that enable this increased load transfer do not reduce the shells' yield strength. For the purposes of the design and potential performance assessments presented here, the SWCNT results will be considered to represent a reasonable best-case scenario for tensile loading. Although this may slightly understate the potential performance of MWCNTs with well-coupled shells, the approximation is justified both by the comparability

between the SWCNT and coupled-shell MWCNT results and by the better-characterized set of assumptions that go into the SWCNT calculations. SWCNTs with small diameters also offer the most stability against radial deformation due to van der Waals interactions when in close contact with other nanotubes [13]. With an applied tensile strain of 15% to 1.02 nm diameter SWCNTs ($A/A_{\text{encl}} = 0.75$), the achievable energy density u_v for a single tube is $8.4 \times 10^6 \text{ kJ m}^{-3}$ (corresponding to a gravimetric energy density u_m of $5 \times 10^3 \text{ kJ kg}^{-1}$), while for a densely packed bundle of these tubes, the maximum volumetric energy density u_v is 9% less, or $7.7 \times 10^6 \text{ kJ m}^{-3}$. In comparison, the volumetric energy density of a lithium-ion battery is in the range of 0.9×10^6 – $1.44 \times 10^6 \text{ kJ m}^{-3}$, corresponding to a gravimetric energy density of 430 – 650 kJ kg^{-1} [18], and the energy density of a steel spring is about 1080 kJ m^{-3} or 0.14 kJ kg^{-1} [19].

When sufficiently large loads are applied to CNTs in bending, torsion or compression, they deform into complex buckling patterns. While the buckles remain largely elastic and reversible [20], loading above the buckling point increases the likelihood of permanent defects forming in the lattice to release the localized strain. Beyond the first buckle, the quadratic relations between strain energy and strain for compression, strain energy and bending angle for bending, and strain energy and twist angle for torsion are lost, and these relations become roughly linear [6, 21]. To avoid permanent defects forming in the lattice and to maintain the more favorable quadratic dependence of stored energy on strain, applying loads sufficient to induce buckling should be avoided when using CNT-based springs for energy storage.

The treatment of CNTs loaded in compression mirrors that of CNTs in tension, with two important differences. First, energy storage in CNTs under compression may be limited by buckling rather than by the elastic limit of the material. Second, as mentioned above, a compressive loading can be transferred to the inner shells of a MWCNT without the need to grasp the inner shells directly. Therefore, equation (4) can be used to calculate the maximum strain energy density in a compressively loaded, MWCNT-based spring without modification.

The critical buckling strain for a CNT depends on its structure and is highly sensitive to the number of shells, the CNT diameter, and for MWCNTs, the type and degree of interaction between adjacent shells. Various analytical models have been created to capture this buckling behavior; two basic models will be used here. In one model, Chang *et al* [22] used molecular mechanics to develop an expression for the critical buckling strain of both SWCNTs and thick MWCNTs in compression, where a ‘thick’ MWCNT is defined as a tightly packed one that has a diameter ratio d_i/d_o of less than 0.62. In this model, the critical buckling strain ϵ_{cr}^s for SWCNTs is calculated as

$$\epsilon_{\text{cr}}^s = \frac{4}{d} \sqrt{\frac{D_o}{Et} \left(1 + \frac{h}{d}\right)}, \quad (5)$$

where d is the SWCNT diameter, $h = 0.34 \text{ nm}$ is the effective wall thickness, $D_o = 0.85 \text{ eV}$ is the bending stiffness and $Et = 360 \text{ J m}^{-2}$ is the in-plane stiffness of the SWCNT. The

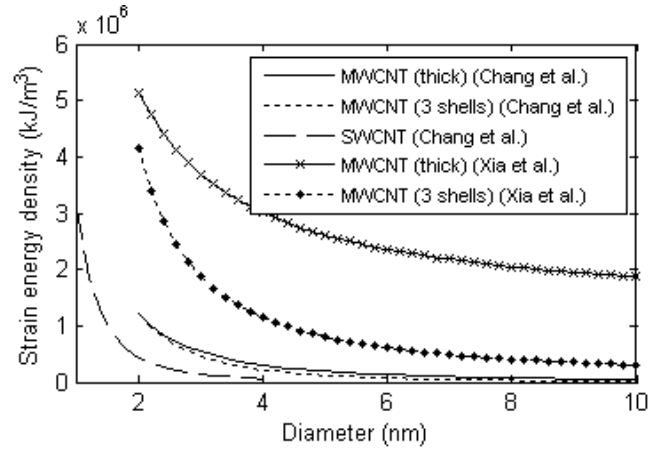


Figure 2. Maximum volumetric energy density before the onset of buckling in compression plotted as a function of diameter for SWCNTs, and plotted as a function of outer diameter for MWCNTs with three shells and for thick MWCNTs.

critical buckling strain ϵ_{cr}^m for thick MWCNTs in compression is found in this model to be insensitive to the inner diameter d_i and depends only on the outer diameter d_o according to

$$\epsilon_{\text{cr}}^m = \frac{0.0985 \times 10^{-9}}{d_o}. \quad (6)$$

In another model, Xia *et al* created a continuum model to predict the onset of buckling in MWCNTs. This model is supported by molecular dynamics simulations and can be used to describe buckling either in ideal MWCNTs or in MWCNTs with inter-shell sp^3 bonding. The critical buckling strain is given in [17] as

$$\epsilon_{\text{cr}}^m = \frac{h}{R\sqrt{3(1-\nu^2)}} + \frac{n-1}{n} \frac{G\delta}{Eh} \quad (7)$$

where R is the average radius of the MWNT, n is the number of shells, ν is the Poisson’s ratio, G is the shear modulus, and δ is the spacing between neighboring shells. Both models yield similar values for the critical buckling strain for ideal MWCNTs.

Calculated maximum strain energy densities for SWCNTs and MWCNTs with various shell structures in compression before the onset of buckling are plotted as a function of diameter in figure 2, using the three models for buckling strain described above. A fraction of inter-shell sp^3 bonds of 6% has been used in the buckling strain model from [17]. The calculations assume in all cases that buckling occurs before the elastic limit is reached, which is valid if the elastic strain limit is greater than ϵ_{cr}^s in the case of SWCNTs and ϵ_{cr}^m in the case of MWCNTs. Independent of the buckling model that is used, energy density decreases rapidly with increasing diameter because of the limit on the applied strain due to buckling. Thick MWCNTs also have higher energy density than thinner MWCNTs and SWCNTs for the same outer diameter because of their dense inner shells and higher buckling strain. Beyond these trends, it can be seen that if CNT deformation is limited only by buckling, the energy

density of MWCNTs with inter-shell bonding is higher than the energy density both of SWCNTs and of MWCNTs with only van der Waals interactions between neighboring shells. These results are valid only if the elastic limit exceeds the buckling limit. Given that the buckling limit for the MWCNTs examined here is calculated to be as high as 0.1 for certain geometries, this assumption may not be valid. If a fraction of the atoms in a MWCNT form inter-wall bonds, the resulting defects may lower the elastic limit of the shells, and consequently MWCNTs containing these defects are more likely to reach their elastic limit before buckling. In that case, the calculations accounting for inter-shell bonding will overestimate the achievable energy density in MWCNTs. In general, the maximum achievable energy density of SWCNTs depends on parameters that are known with a greater degree of certainty than those of MWCNTs. SWCNTs are therefore recommended as a better structure than MWCNTs for a spring in compression because their smaller diameters ensure high energy densities, independent of the details of the inter-shell interaction.

To evaluate the validity of the continuum beam model employed here for a single shell, the strain energy per atom of a SWCNT under uniform compressive loading prior to buckling is compared with the results of molecular mechanics and finite element models. Figure 3 plots strain energy per atom as a function of strain for a 1.41 nm diameter (18, 0) SWCNT modeled by Arroyo *et al* [23], a 1.25 nm diameter (16, 0) SWCNT modeled by Sears *et al* [24], and a 1 nm diameter (7, 7) SWCNT modeled by Yakobson *et al* [21]. In general, strain energy is expected to be largely independent of chirality [1]. Strain energy per atom for each modeled SWCNT is plotted up to its respective compressive buckling strain, which varies between models because of the different diameters of the modeled SWCNTs in addition to variations between models. The energy per atom of a SWCNT predicted by the continuum beam model is plotted as a function of strain on the same graph. The energy predicted by the continuum beam model is independent of diameter and chirality, so the curve is plotted up to the maximum strain on the graph since the SWCNT diameter, which determines the buckling strain, is unspecified. Good agreement between the four models indicates that the continuum beam model can be used to obtain reasonable energy density estimates.

Inter-shell sp³ bonding will be neglected in determining the onset of buckling in MWCNTs subjected to bending or torsional loads, for which the analytical expressions of [17] are not directly applicable; the models from [21, 22, 25] will be used instead. As in the case of compression, inter-shell sp³ bonds are expected to increase the buckling strain of MWCNTs but adversely affect the elastic limit. The range of potential MWCNT inter-shell interactions and the variations among the models that describe the onset of buckling in CNTs add some uncertainty to the maximum predicted strain energy densities. The assumptions used here nonetheless provide a reasonable estimate of the overall maximum strain energy density, with a degree of variation with detailed shell structure that is similar to that observed for compressed CNTs.

The treatment of energy storage in bending requires a different framework because of the spatial variation of strain

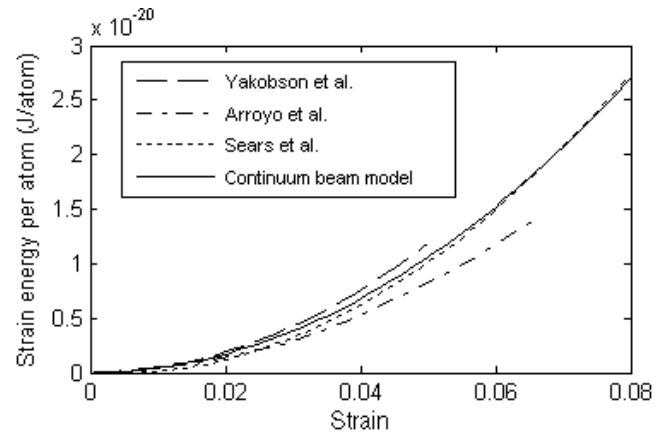


Figure 3. Strain energy per atom of a CNT under compression calculated using the continuum beam model compared to the results of molecular dynamics [21, 24] and finite element [23] models.

within a bent CNT. In pure bending, a uniform bending moment is applied to the cylindrical beam so that it develops a maximum strain of $\pm\epsilon$ at its outer diameter. The volumetric strain energy density of the beam is

$$u_v = \frac{1}{8} E \epsilon^2 \left[1 - \left(\frac{r_i}{r_o} \right)^4 \right]. \quad (8)$$

For a given value of ϵ , high energy density can be achieved when the ratio r_i/r_o of the CNT is small, which implies that the highest energy densities will be achieved in SWCNTs with small outer diameters or in MWCNTs with densely packed shells. The amount of bending that can be applied to a CNT is limited by the strain at which a CNT begins to buckle. Yakobson *et al* [21] modeled the critical buckling strain of a SWCNT under bending as

$$\epsilon_{cr}^s = \frac{0.077 \times 10^{-9}}{d}, \quad (9)$$

where d is the SWCNT diameter. Chang *et al* [22] modeled the critical buckling strain of thick MWCNTs in bending as

$$\epsilon_{cr}^m = \frac{0.111 \times 10^{-9}}{d_o + h}, \quad (10)$$

where d_o is the outer diameter and $h = 0.34$ nm. Both expressions contain an inverse relation between buckling strain and diameter. As for the case of compressive loading, deforming a CNT in pure bending has the advantage of deforming all shells of a MWCNT rather than just the outermost shell, leading to higher overall energy density than if only the outermost shell were deformed.

The maximum overall volumetric strain energy density in bending before the onset of buckling is plotted as a function of diameter in figure 4. Energy density decreases rapidly with increasing diameter because of the decrease in buckling strain at higher diameters. For the same outer diameter, MWCNTs store energy with higher density than SWCNTs because of the dense packing of inner shells. However, SWCNTs generally have smaller diameters than MWCNTs, so SWCNTs will tend

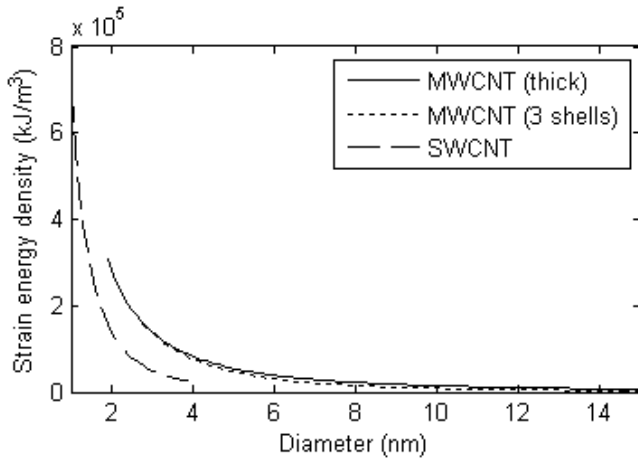


Figure 4. Maximum volumetric strain energy density before the onset of buckling in bending plotted as a function of diameter for SWCNTs, and as a function of outer diameter for MWCNTs with three shells and for thick MWCNTs.

to store energy with higher density, although modifications to the critical buckling strain of MWCNTs due to strong inter-shell interactions may improve the performance of MWCNTs. Overall, SWCNTs with small diameters would be an excellent structure for a spring deformed in bending. Typical radii of curvature for bent CNTs at the onset of buckling are 6.7 and 26 nm for 1.02 and 2 nm diameter SWCNTs respectively, which are quite small for implementation in springs at anything above the nanoscale.

To estimate the maximum strain energy density of a CNT under torsion, a torsional moment M is applied to the cylindrical beam. The volumetric strain energy density u_v , is given by

$$u_v = \frac{M^2}{2GJ\pi r_o^2}, \quad (11)$$

where G is the shear modulus and $J = \frac{\pi}{2}(r_o^4 - r_i^4)$ is the polar moment of inertia of the beam. Wang *et al* [25] propose a model for the critical moment at which buckling first occurs for torsionally loaded long SWCNTs and MWCNTs:

$$M_{cr} = \frac{4EJh^{3/2}}{3(r_o + r_i)^{5/2}(1 - \nu^2)^{3/4}}, \quad (12)$$

where ν is the Poisson's ratio. For ideal MWCNTs, an applied moment affects only the outer shell since grasping the inner shells is difficult [16, 26]. However, previous work has shown that load transfer in torsion may be increased through inter-wall sp³ bonding [27], which would enable inner shells to contribute to supporting a torsional load. Using the critical moment from [25], the maximum volumetric energy density of torsionally loaded SWCNTs and MWCNTs before the onset of buckling is calculated and plotted against diameter in figure 5, indicating that the maximum energy density decreases rapidly with increasing diameter. In this plot, the inner shells of the MWCNTs are assumed to carry loads. However, if only the outer shell of a MWCNT supported an applied load, then the curves for MWCNTs would coincide with the curve for SWCNTs. Within these approximations, SWCNTs will have

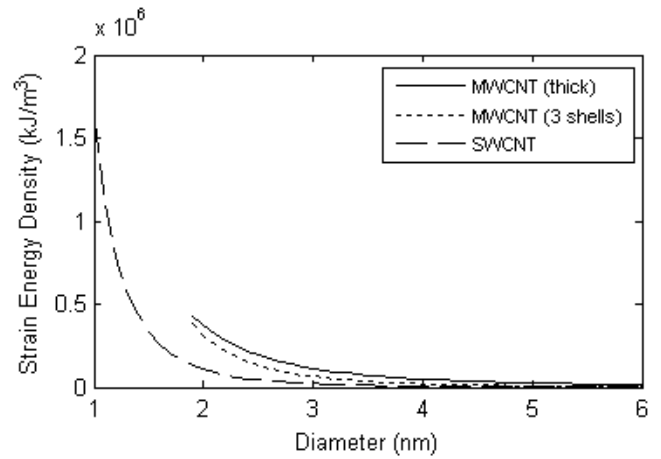


Figure 5. Maximum volumetric energy density before the onset of buckling in torsion as a function of diameter for SWCNTs and outer diameter for MWCNTs.

a higher volumetric energy density than MWCNTs because of their smaller outer diameters, so that for energy storage in pure torsion, the highest energy densities are achieved in SWCNTs with small diameters. For stronger inter-shell interactions, the energy density stored in MWCNTs will be higher than the MWCNT strain energy density shown here only if the increased critical buckling strain is less than the elastic limit which may be affected by the defects present in the structure. Nonetheless, MWCNTs with inter-shell bonding may once again offer an alternative to SWCNTs as a means of reaching high strain energy density.

There are advantages and disadvantages to each deformation mode and type of CNT structure. Deforming MWCNTs in axial tension or torsion comes with the challenge of grasping the inner shells, while compression and bending ensure that loading is applied to all shells. Torsion, bending and compression are limited by critical buckling stresses, while tension is limited only by the stress at the elastic limit. For all loadings, the highest energy density without strong inter-shell bonding is achieved in SWCNTs with diameters of 2 nm or less, with MWCNTs with strong inter-shell bonding offering a potentially attractive alternative structure.

The strain energy densities of bundles of SWCNTs deformed in each of the four deformation modes as a function of diameter are plotted in figure 6. The plot shows that storing energy in tension is advantageous for SWCNTs with diameters greater than 2 nm since the maximum energy density before the onset of buckling drops off rapidly in compression, bending, and torsion because of the limits on the applied strain due to buckling. For diameters smaller than 2 nm, the energy densities of all deformation modes are in the same range, so any of the deformation modes could be selected for a spring, based on practical considerations of implementation. Nevertheless, if elastic strains of 9% or greater can be applied to CNTs in tension before failure, then tension would be the best choice regardless of diameter. These results indicate that a good choice for a spring would be a dense bundle of SWCNTs with diameters less than 2 nm, stretched in tension.

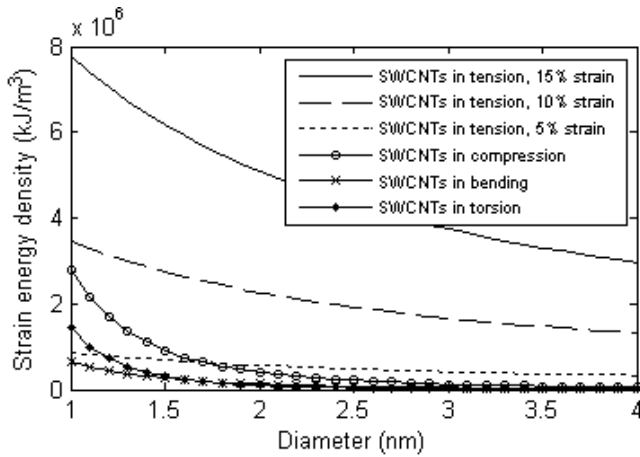


Figure 6. Maximum volumetric energy density of SWCNT bundles as a function of diameter for four deformation modes.

A support structure is needed to deform a CNT-based spring and hold it in its maximally deformed configuration until the stored energy is released. The volume and mass of this structure must be included in system-level energy density calculations. For instance, a support structure in compression may be used to maintain a bundle of CNTs in tension, and since there are no materials as strong in compression as carbon nanotubes are in tension, the supporting structure must be larger than the CNT-based spring itself. This will reduce the overall system's energy density considerably.

One type of support structure is a solid cylindrical shaft around which a CNT spring stretched predominantly in tension is wrapped. While the loaded support structure stores energy itself, we conservatively assume that only the energy from the spring can be extracted to perform useful work, and the energy stored in the support structure is neglected when calculating the overall energy density of the combined spring and support system. In practice, an architecture could be designed in which the energy in the support structure is used to perform work as well, so it may be possible to reach higher energy densities than the ones proposed here.

The maximum volumetric energy density in the combined spring and support structure consisting of a cylindrical shaft about which the CNT is wrapped, as described above, is [14]

$$u_v = \frac{E\varepsilon^2 A/A_{\text{encl}}}{2 + \frac{E\varepsilon}{\sigma_y}}, \quad (13)$$

where σ_y is the compressive yield strength of the support structure material, and all the other symbols are defined as above. The corresponding maximum volumetric energy density for a CNT spring supported in pure tension combined with a compressively loaded support is [14]

$$u_v = \frac{\frac{1}{2}E\varepsilon^2}{\frac{A_{\text{encl}}}{A} + \frac{E\varepsilon}{\sigma_y}}. \quad (14)$$

A comparison of equations (13) and (14) indicates that higher energy density in a supported CNT spring can be reached with a circular shaft support than with a support in axial

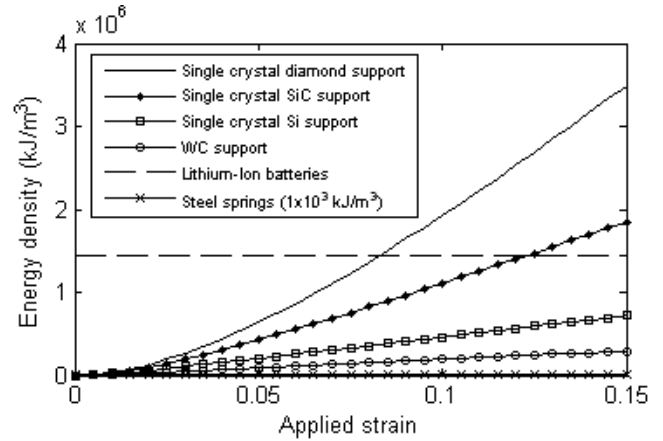


Figure 7. Volumetric energy densities of bundles of SWCNTs under tensile loading with a cylindrical shaft support structure made of single crystal diamond, silicon, silicon carbide and tungsten carbide. The energy densities of conventional energy storage technologies (lithium-ion batteries and steel springs) are also shown on the graph for comparison.

compression, though the difference in performance between the two support structures is relatively small.

The energy density of a bundle of 1.02 nm diameter SWCNTs under tensile loading is plotted as a function of applied strain in figure 7, taking into account a cylindrical shaft support structure. The materials considered for the support structure are single crystal silicon ($\sigma_y = 7$ GPa), single crystal silicon carbide ($\sigma_y = 21$ GPa), hot-pressed SiC-N ($\sigma_y = 7$ GPa), single crystal diamond ($\sigma_y = 53$ GPa), and tungsten carbide ($\sigma_y = 2.7$ GPa), all chosen for their high compressive strength [28, 29]. The choice of material for the support structure is important because its properties have an impact on the resulting energy density. The energy densities of lithium-ion batteries and steel springs are plotted on the same graph for comparison. The maximum achievable overall stored energy density is predicted to be comparable to lithium-ion batteries as long as high elastic strains can be applied to the CNTs and a high quality material is used for the support structure. A CNT spring with its associated support structure can store energy with a density more than two orders of magnitude greater than steel springs, so CNT springs have the potential to significantly improve upon the energy storage capability of currently available mechanical springs.

These analytical models represent a computationally efficient approach to assessing the potential value of CNT springs and guiding decisions about their design. Characterizing and reaping the full benefits of the CNT spring technology will also require experimental characterization of CNT springs. Experiments on first generation carbon nanotube springs have been done, and both their execution and their results are reported in detail elsewhere [30]. In these experiments, energy storage in fibers made of continuous, aligned, four-shelled MWCNTs was measured using cyclic tensile loading tests. The gravimetric energy density of the CNT fibers exceeds the gravimetric energy density of steel springs by a factor of more than 30, indicating the considerable advantage of CNTs over conventional materials such as steel

for mechanical springs. The volumetric energy density for the first generation CNT fibers falls short of the energy density of mechanical springs by a factor of about 5 in part because non-ideal packing of the CNTs within the initial fibers resulted in lower than ideal densities. The results reported in [30] do not match the theoretically predicted upper bounds on energy densities as found here of $7.7 \times 10^6 \text{ kJ m}^{-3}$ or $5 \times 10^3 \text{ kJ kg}^{-1}$ for defect-free SWCNT groupings with ideal packing at 15% strain. The results are also lower than the predicted ideal energy density for MWCNTs comparable to those used in the experiments of $4.7 \times 10^6 \text{ kJ m}^{-3}$ if all shells share the applied load, or $1.3 \times 10^6 \text{ kJ m}^{-3}$ if only the outer shell supports the load. Nonetheless, the results do represent a significant advance over steel spring technology. The reasons for the difference between the maximum theoretical and experimental values include a number of experimental non-idealities in the first generation CNT springs and test apparatus which are discussed at length in [30].

3. Conceptual design and modeling of a CNT spring-based power source

One could construct practical systems in which small or large CNT springs power different-sized mechanical or electrical loads. For the case of a mechanical load, the spring may be coupled to the load relatively directly, through an appropriate mechanical coupling mechanism. For an electrical load, the energy must also be converted from the mechanical to the electrical domain. As an example of the latter, we now consider the case of using a small CNT-based spring to drive an electrical generator, thus forming an electrical power supply.

On its own, a spring stores potential energy when an external force is applied, but the energy is released in a single rapid burst once the force is removed. An effective power supply must not only store energy over a period of time, but also release the energy only as needed and at the desired power level. One way to slow the rate of energy release from a mechanical spring is to use an escapement mechanism, much like that which has been used in mechanical clocks for centuries. The mechanical work done by the spring as it unwinds may be converted into an electric output by adopting the technology of vibrational energy harvesters; in this case, the mechanical energy comes from a spring rather than from vibrations in the environment. A specific architecture based on these ideas is developed below and used to assess the tradeoffs that arise in such a system. This approach keeps the average power output roughly constant over most of the discharge period, instead of falling steadily as it would if the spring were used to drive a conventional electromagnetic generator connected to a constant electrical load.

This microscale power supply was introduced in [14] as a tool to study how densely energy might be stored in an actual device based on the mechanical deformation of CNTs and how efficiently the energy could subsequently be recovered as an electrical output. A theoretical model of the system was built to simulate the system's performance, and the simulation results are used to determine how scaling affects the power output, overall system efficiency, operating frequency of the

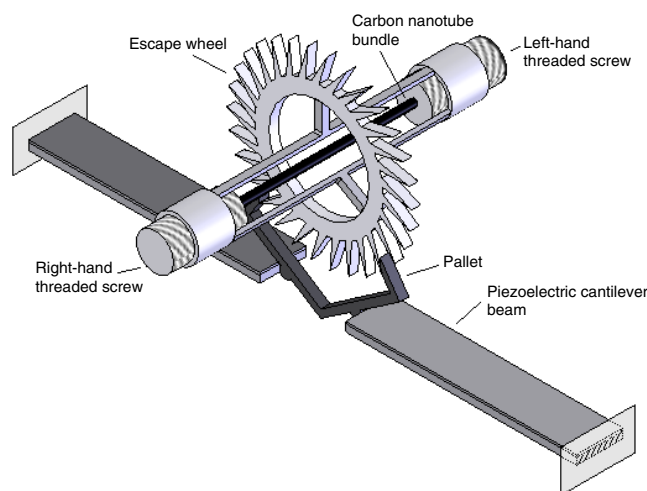


Figure 8. Schematic diagram of a power supply that stores energy in a CNT-based spring, showing the spring stretched between a right- and left-handed pair of screws, the escape wheel driven to rotate by the screws, the pallet that is made to oscillate by the escape wheel, and the two piezoelectric cantilever beams with which the pallet interacts.

energy regulation mechanism, and energy discharge time. The conceptual design presented here employs components that are chosen for simplicity of operation and ease of modeling rather than for microfabricatability, and it has not been systematically optimized for performance. Thus this design should not be viewed as a blueprint for a practical device nor should the results be viewed as a best-case estimate of how well such a device could perform. Nevertheless, the results do provide a lower bound on the performance of a practical device, which complements the more general upper bounds obtained in section 2.

For the escapement mechanism, a dead beat escapement was adopted; this escapement is commonly used in pendulum clocks and is well understood [31]. In this mechanism, an escape wheel (a gear with an application-specific tooth design) is driven to rotate by the force from a spring (a mainspring in horology). Without any additional mechanisms, the escape wheel would accelerate and release all of the energy from the spring in a single burst. A second component called a pallet is employed to control the rate of energy release from the spring through the escape wheel. The pallet is connected to a pivot and is driven to oscillate by a second spring (a hairspring in horology). Each oscillation of the pallet allows the toothed escape wheel to rotate by an angle equal to the angular spacing between two teeth. The escape wheel transfers energy to the oscillating spring on each increment of rotation, so that the amplitude of the oscillations remains large over time despite damping losses. The oscillations of the pallet in turn drive a vibrational energy harvester, as described below.

Figure 8 shows a schematic diagram of this power supply. The energy storage element is modeled as a defect-free densely packed assembly of parallel SWCNTs with a stiffness of 1 TPa and ideal strength. This CNT grouping is connected between a right-handed screw and a left-handed screw. The attachment is assumed to distribute the load evenly among all

tubes within the grouping and is assumed to be sufficiently strong to withstand the force from the fully stretched spring without fracture occurring at the points of attachment. Energy is stored in the system by turning both screws in the same direction, thereby stretching the CNT bundle in pure extension. Once the spring is fully stretched, the energy is maintained in the system by latching the two screws in place. During operation, a separate mechanism allows the escape wheel to spin while preventing the screws from doing so. The force from the spring acting on the screw threads of the escape wheel makes it spin. As the escape wheel spins, the spring contracts. Each pallet oscillation allows the escape wheel to advance by a small increment, which in turn constrains the spring to contract by only a small increment with each pallet oscillation. The motion of the pallet drives a pair of identical cantilever beams that oscillate at their resonant frequency and have a phase difference of 180°. A thin film of piezoelectric material on the cantilevers is used to convert the mechanical oscillations into electrical energy.

The spring is assumed to be a bundle of parallel SWCNTs with a circular cross-section and bundle radius b stretched under axial tension to a fully reversible 6% strain. Treating each SWCNT as a hollow cylinder of thickness 0.34 nm, the elastic strain energy stored in the spring is

$$U = \frac{1}{2} E \varepsilon^2 \pi b^2 f \frac{A}{A_{\text{encl}}} L \quad (15)$$

where $E = 1$ TPa is the usual Young's modulus of an SWCNT, ε is the applied strain, $f = 91\%$ is the fill factor for ideal hexagonal close packing, L is the length of the bundle, and $A/A_{\text{encl}} = 0.75$ for SWCNTs with diameters of 1.02 nm.

The spring, escapement mechanism and piezoelectric cantilevers are analogous to a driven damped oscillator, but with the important difference that the driving force from the spring depends on the angle of the escape wheel rather than on time directly [31]. The angle of rotation of the pallet with respect to its neutral position is denoted θ_p , and the angle of rotation of the escape wheel with respect to its starting position is denoted θ_w . With this particular escapement design, the escape wheel rotates and the spring contracts for $-3^\circ < \theta_p < 3^\circ$. For $\theta_p > 3^\circ$ and $\theta_p < -3^\circ$, the escape wheel is locked in place and the pallet oscillates freely. The equation of motion describing the cantilever tip displacement $x(t)$ is

$$m_{\text{eff}} \ddot{x} + (b_m + b_e) \dot{x} + kx = -I_p \ddot{\theta}_p \frac{\cos(\theta_o + \theta_p)}{e} + u(\theta_p) [M(\theta_w) - I_w \ddot{\theta}_w] \frac{\cos(\theta_o + \theta_p)}{e}, \quad (16)$$

where $u(\theta_p) = 1$ and $\ddot{\theta}_w = \ddot{\theta}_p$ for $-3^\circ < \theta_p < 3^\circ$, and $u(\theta_p) = 0$ and $\dot{\theta}_w = 0$ otherwise. In this equation, m_{eff} is the effective mass of a cantilever beam, b_m is the mechanical damping coefficient, b_e is the electrical damping coefficient, k is the cantilever spring constant, I_w is the moment of inertia of the escape wheel, I_p is the moment of inertia of the pallet, e is the escape wheel radius, and $M(\theta_w)$ is the driving moment on the escape wheel from the spring, including the effects of friction in the screws. Operation begins with the spring in its fully stretched state and ends once the spring has returned to its

Table 1. System dimensions.

	Micron-scale	Submillimeter-scale	Millimeter-scale
Spring diameter	3 μm	30 μm	300 μm
Spring length	8 mm	8 cm	80 cm
Cantilever length	400 μm	4 mm	4 cm
Cantilever width	80 μm	800 μm	8 mm
Cantilever height	20 μm	200 μm	2 mm
Escape wheel radius	50 μm	500 μm	5 mm
Piezoelectric layer thickness	0.5 μm	5 μm	50 μm

original length and all of the energy transferred to the cantilever beams has been converted into electrical energy or dissipated to friction.

The electrical damping coefficient is calculated as $b_e = 2m\zeta_e\omega$ [32], where ζ_e is the electrical damping ratio

$$\zeta_e = \frac{\omega k_{31}^2}{\sqrt{\omega^2 + 1/(RC)^2}}. \quad (17)$$

C is the capacitance of the piezoelectric layer, R is the external load resistance, and ω is the angular frequency of the cantilever oscillations. The electrical damping coefficient depends on the parameters of the electrical circuit and the load driven by the generator, so a suitable circuit can be designed by choosing an appropriate load resistance to adjust the value of b_e . A range of values for the electrical damping coefficient is considered by varying the magnitude of the external load resistance driven by the piezoelectric circuit. The mechanical damping coefficient b_m cannot be known precisely without measuring the performance of the actual system, but it can be approximated using values for the quality factor of cantilever beams reported in the literature.

Using a commonly employed general model (see for example [33]), the electrical power generated by a single piezoelectric cantilever beam is taken to be equal to the power removed from the mechanical system due to the electrical damping:

$$P = \frac{1}{2} b_e \dot{x}^2. \quad (18)$$

Since there are two cantilever beams, the total output power is multiplied by two. Once energy is stored in the spring, three main sources of losses reduce the amount of energy that can be extracted from the system: frictional losses in the screws, losses inherent to the escapement mechanism, and losses in the piezoelectric energy conversion. The overall efficiency of the system η over its discharge time is expressed as:

$$\eta = \frac{2 \int_{t_{\text{start}}}^{t_{\text{end}}} \frac{1}{2} b_e \dot{x}^2 dt}{U}. \quad (19)$$

Based on this analysis, a model of the conceptual power source was generated and simulations were run for systems at different size scales to demonstrate the effect of scaling on the stored energy, the operating frequency, the power output, the discharge time and the efficiency. Three main cases are considered, by scaling all dimensions by factor of 10 in each

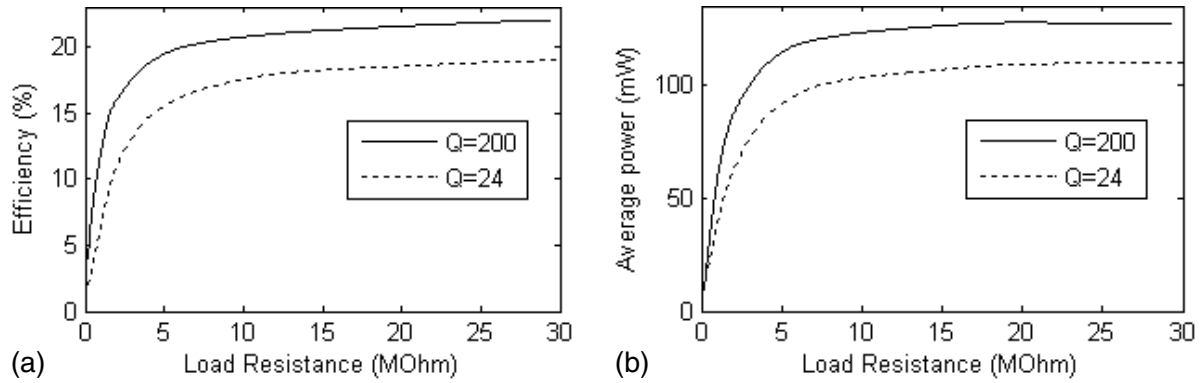


Figure 9. (a) Overall system efficiency and (b) average electric power output versus load resistance for the submillimeter-scale case.

Table 2. Mechanical damping coefficients b_m corresponding to $Q = 24$ and 200.

	Micron-scale	Submillimeter-scale	Millimeter-scale
$Q = 24$ (kg s^{-1})	0.000 04	0.004	0.4
$Q = 200$ (kg s^{-1})	0.000 0045	0.000 45	0.045

Table 3. Operating parameters.

	Micron-scale	Submillimeter-scale	Millimeter-scale
Stored energy (J)	6×10^{-5}	0.06	60
Operating frequency (Hz)	192 700	19 400	1906
Max overall efficiency (%)	22	22	22
Percentage CNTs by mass (%)	0.36	0.36	0.36
Average power output (W)	0.0013	0.13	13
Discharge time (s)	0.01	0.1	1

case, and they are referred to for simplicity as the micron-scale, submillimeter-scale, and millimeter-scale cases. The dimensions of the three systems are listed in table 1.

Appropriate values of b_m are selected by considering mechanical damping coefficients that yield quality factor (Q) values of 24 and 200, values that have previously been reported in the literature for cantilevers that are used as piezoelectric generators [34, 35]. The values of b_m are listed in table 2. The electrical damping ratio ζ_e is varied by considering a range of values for the load resistance in order to vary the electrical damping coefficient b_e . Operating parameters are listed for the three cases in table 3. Plots are generated of efficiency and power output versus load resistance for the three systems.

The operating frequencies of the representative devices are 190 kHz for the micron-scale system, 19 kHz for the submillimeter-scale system and 1.9 kHz for the millimeter-scale system. These results show that the operating frequency of the system scales roughly inversely with the overall scale of the system, as expected. Figure 9(a) shows a plot of efficiency versus load resistance for the submillimeter-scale case. Similar plots were generated for the other two cases. In all three cases,

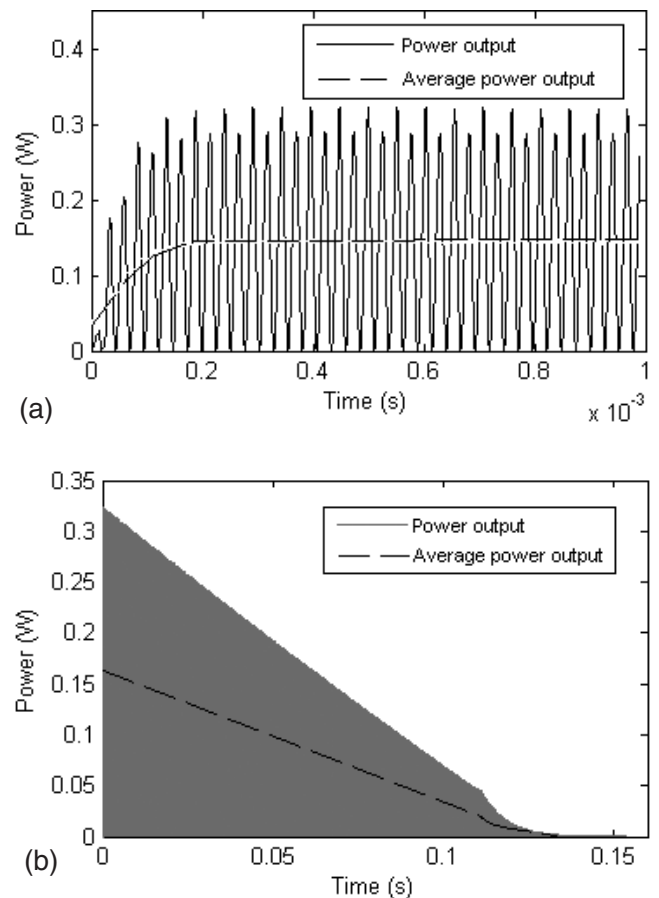


Figure 10. Electric power output versus time for the submillimeter-scale case with $b_m = 0.004$ and $b_e = 0.01 \text{ kg s}^{-1}$, showing (a) detailed variation of the power over short times and (b) power variation over the entire discharge time.

overall efficiency approaches 18% with a Q of 24 and 22% with a Q of 200. As expected, greater efficiencies can be reached with higher values of Q . These results indicate that efficiency is unaffected by the scale of the system within the limits of this model.

Average power output is defined as the average power output over the discharge time. Average power output is plotted against load resistance for the submillimeter-scale case in figure 9(b). A plot of power output versus time is shown

in figure 10 for the submillimeter-scale case with $b_m = 0.004$ and $b_e = 0.01 \text{ kg s}^{-1}$. Power reaches 0.13 W with a Q of 200 and a discharge time of 0.1 s. As expected, power output is higher with larger values of Q due to the higher efficiency of the energy conversion. Similar plots were generated for the micron-scale and millimeter-scale systems. Power output reaches 0.0013 W with a discharge time of 0.01 s in the micron-scale case, and 13 W for the millimeter-scale case with a discharge time of 1 s. The discharge time of the spring scales roughly linearly with the linear dimensions of the spring. Energy storage scales cubically with the linear dimensions (linearly with spring volume), so power output scales as the square of the spring's linear dimensions.

4. Conclusions

We have shown that springs comprised of highly ordered bundles of parallel carbon nanotubes form the basis for a new class of energy storage devices. These devices are physically quite different from other kinds of energy storage devices based on carbon nanotubes, such as supercapacitor electrodes [36] or hydrogen adsorbents for use with fuel cells [37]. Like supercapacitors, such devices have the potential to be discharged and recharged rapidly, repeatedly and safely even at extreme temperatures, but they also have the potential to achieve energy densities and self-discharge rates comparable to electrochemical batteries and perhaps even approaching those of fuel cell-based systems.

Considering the carbon nanotube (CNT) spring element alone, calculations using the widely accepted Young's modulus and yield strains for CNTs predict the maximum energy density of CNT springs loaded in tension at the highest applied strains to be 7000 times greater than that of steel springs and eight times greater than the energy density of lithium-ion batteries. Once practical considerations are taken into account, such as the need for a support structure or additional extraction hardware, the energy density of a power source containing a CNT spring will be lower than the calculations predict for the spring element alone. However, even when a support structure is taken into consideration, a CNT spring can still store energy with a density more than two orders of magnitude higher than a steel spring and on the same level as batteries. Groupings of SWCNTs with diameters of 2 nm or smaller stretched in tension are identified as the best structure and loading mechanism for high-performance springs.

The conceptual power supply model presented in this paper provides only an early stage mathematical examination of the concept; it has not yet been optimized for performance or manufacturability. The results of this work indicate that operating frequency, efficiency, discharge time and power all scale reasonably with size, leaving flexibility in the choice of overall size scale. It is important to observe that at all three size scales presented here, the CNT-based energy storage element occupies a small fraction of the mass and volume of the total system. The model does not yet demonstrate the extent to which systems can be engineered to maintain high overall energy density. Future work should concentrate on optimizing the fraction by mass and volume of CNTs in a power source.

Acknowledgments

The authors would like to thank Jonathan Leavitt for many useful discussions, John Hart for providing the carbon nanotube samples, the MIT Institute for Soldier Nanotechnologies for the use of their testing facilities, and the Deshpande Center for Technological Innovation, the MIT Energy Initiative, and NSERC for their financial support of this work.

References

- [1] Qian D, Wagner G J, Liu W K, Yu M and Ruoff R S 2002 Mechanics of carbon nanotubes *Appl. Mech. Rev.* **55** 495–533
- [2] Walters D A, Ericson L M, Casavant M J, Liu J, Colbert D T, Smith K A and Smalley R E 1999 Elastic strain of freely suspended single-wall carbon nanotube ropes *Appl. Phys. Lett.* **74** 3803–5
- [3] Liew K M, Hea X Q and Wong C H 2004 On the study of elastic and plastic properties of multi-walled carbon nanotubes under axial tension using molecular dynamics simulation *Acta Mater.* **52** 2521–7
- [4] Meo M and Rossi M 2007 A molecular-mechanics based finite element model for strength prediction of single wall carbon nanotubes *Mater. Sci. Eng. A* **454/455** 170–7
- [5] Yakobson B I, Campbell M P, Brabec C J and Bernholc J 1997 High strain rate fracture and C-chain unraveling in carbon nanotubes *Comput. Mater. Sci.* **8** 341–8
- [6] Arroyo M and Belytschko T 2005 Continuum mechanics modeling and simulation of carbon nanotubes *Meccanica* **40** 455–69
- [7] Saito R, Dresselhaus G and Dresselhaus M S 1998 *Physical Properties of Carbon Nanotubes* (London: Imperial College Press)
- [8] Salvétat J, Bhattacharyya S and Pipes R B 2006 Progress on mechanics of carbon nanotubes and derived materials *J. Nanosci. Nanotechnol.* **6** 1857–82
- [9] Atkinson K R et al 2007 Multifunctional carbon nanotube yarns and transparent sheets: fabrication, properties, and applications *Physica B* **394** 339–43
- [10] Koziol K J V, Moysala A, Motta M, Cunniff P, Sennett M and Windle A 2007 High-performance carbon nanotube fiber *Science* **318** 1892–5
- [11] Zheng L X et al 2004 Ultralong single-wall carbon nanotubes *Nat. Mater.* **3** 673–6
- [12] Zhang X et al 2007 Ultrastrong, stiff, and lightweight carbon-nanotube fibers *Adv. Mater.* **19** 4198–201
- [13] Pantano A, Parks D M and Boyce M C 2004 Mechanics of deformation of single- and multi-wall carbon nanotubes *J. Mech. Phys. Solids* **52** 789–821
- [14] Hill F A 2008 Energy storage in carbon nanotube super-springs *SM Thesis* Massachusetts Institute of Technology
- [15] Qian D, Liu W K and Ruoff R S 2003 Load transfer mechanism in carbon nanotube ropes *Compos. Sci. Technol.* **63** 1561–9
- [16] Yu M, Lourie O, Dyer M J, Moloni K, Kelly T F and Ruoff R S 2000 Strength and breaking mechanism of multiwalled carbon nanotubes under tensile load *Science* **287** 637–40
- [17] Xia Z H, Guduru P R and Curtin W A 2007 Enhancing mechanical properties of multiwall carbon nanotubes via sp^3 interwall bridging *Phys. Rev. Lett.* **98** 245501
- [18] Tarascon J M and Armand M 2001 Issues and challenges facing rechargeable lithium batteries *Nature* **414** 359–67
- [19] Madou M 2002 *Fundamentals of Microfabrication* (Boca Raton, FL: CRC Press)
- [20] Falvo M R, Clary G J, Taylor R M, Chi V, Brooks F P, Washburn S and Superfine R 1997 Bending and buckling of carbon nanotubes under large strain *Nature* **389** 582–4

- [21] Yakobson B I, Brabec C J and Bernholc J 1996 Nanomechanics of carbon tubes: instabilities beyond linear response *Phys. Rev. Lett.* **76** 2511–4
- [22] Chang T, Guo W and Guo X 2005 Buckling of multiwalled carbon nanotubes under axial compression and bending via a molecular mechanics model *Phys. Rev. B* **72** 064101
- [23] Arroyo M and Belytschko T 2004 Finite element methods for the non-linear mechanics of crystalline sheets and nanotubes *Int. J. Numer. Methods Eng.* **59** 419–56
- [24] Sears A and Batra R C 2004 Macroscopic properties of carbon nanotubes from molecular-mechanics simulations *Phys. Rev. B* **69** 235406
- [25] Wang Q, Quek S T and Varadan V K 2007 Torsional buckling of carbon nanotubes *Phys. Lett. A* **367** 135–9
- [26] Papadakis S J, Hall A R, Williams P A, Vicci L, Falvo M R, Superfine R and Washburn S 2004 Resonant oscillators with carbon-nanotube torsion springs *Phys. Rev. Lett.* **93** 146101
- [27] Hai-Yang S and Win-Wei Z 2009 Molecular dynamics study of effects of sp³ interwall bridging upon torsion behavior of double-walled carbon nanotube *Phys. Lett. A* **373** 682–5
- [28] Petersen K E 1982 Silicon as a mechanical material *Proc. IEEE* **70** 420–57
- [29] Wang H and Ramesh K T 2004 Dynamic strength and fragmentation of hot-pressed silicon carbide under uniaxial compression *Acta Mater.* **52** 355–67
- [30] Hill F A, Havel T F, Hart A J and Livermore C 2009 Storing elastic energy in carbon nanotubes *J. Micromech. Microeng.* at press
- [31] Kesteven M 1978 On the mathematical theory of clock escapements *Am. J. Phys.* **46** 125–9
- [32] Roundy S, Wright P K and Rabaey J 2003 A study of low level vibrations as a power source for wireless sensor nodes *Comput. Commun.* **26** 1131–44
- [33] Jeon Y B, Sood R, Jeong J H and Kim S G 2005 MEMS power generator with transverse mode thin film PZT *Sensors Actuators A* **122** 16–22
- [34] Cho J H, Richards R F, Bahr D F, Richards C D and Anderson M J 2006 Efficiency of energy conversion by piezoelectrics *Appl. Phys. Lett.* **89** 104107
- [35] Richards C D, Anderson M J, Bahr D F and Richards R F 2004 Efficiency of energy conversion for devices containing a piezoelectric component *J. Micromech. Microeng.* **14** 717–21
- [36] Schindall J 2007 The charge of the ultracapacitors *IEEE Spectr.* **44** 42–6
- [37] Dillon A C, Jones K M, Bekkedahl T A, Kiang C H, Bethune D S and Heben M J 1997 Storage of hydrogen in single-walled carbon nanotubes *Nature* **386** 377–9